Supporting Information

Modeling Morphology and Catalytic Activity of Nanoparticle Ensembles Under Reaction Conditions

Raffaele Cheula[a][b], Matteo Maestri*[a] and Giannis Mpourmpakis**[b]

[a] *Laboratory of Catalysis and Catalytic Processes, Dipartimento di Energia, Politecnico di Milano, Via La Masa, 34, 20156, Milano, Italy.*

[b] *Department of Chemical and Petroleum Engineering, University of Pittsburgh, 4200 Fifth Avenue, 15260, Pittsburgh, PA, USA.*

* email: matteo.maestri@polimi.it

** email: gmpourmp@pitt.edu

Table of Contents

Section 1: Creation of the ensemble of nanoparticles.

Single-crystal fcc nanoparticles are created cutting the bulk phase with 8 Miller-index planes: (100), (110), (111), (210), (211), (311), (321), (331). The construction is centered on each symmetry points of the irreducible Brillouin zone.

Each of the 5 subsections of decahedral nanoparticles are cut with 5 different planes: (111) is the plane which cut the top and bottom surfaces of the particle creating (111)-like surfaces, (111)', (100) and (311) cut the lateral surfaces and (111)'' creates the hole at the top and bottom of the particle.

Each of the 20 subsection of icosahedra nanoparticles are cut with 3 planes: (111), (211) and (311), which create islands (and low-symmetry peninsulas) of atoms on (111)-like surfaces with different dimensions.

The number of nanoparticles created depends on the size of the initial ensemble of shapes, which is controlled by the number of planes chosen and the threshold value for the difference in distance between the planes. Moreover, it depends on the number of atoms removed in each iteration of the second step of the procedure. It is necessary to assess whether the number of nanoparticles of the ensemble is high enough to represent a large diversity of shapes. To this aim, we increase the maximum distance between different planes and the number of atoms removed in each iteration of step two of the procedure and we repeat the whole analysis, finding negligible variations in the final results.

The library of scripts employed in this work is available at the Github page:

github.com/raffaelecheula/nanoparticles_ensembles.

Section 2: Model for Gibbs free energy of formation of Rh nanoparticles in the presence of CO.

The cohesive energy of bulk Rh is calculated as difference between the DFT energy of one Rh atom in the fcc crystal cell and the DFT energy of a single Rh atom in vacuum:

$$E_{coh}^{bulk} = E_{DFT}^{bulk}/N_{Rh}^{bulk} - E_{DFT}^{gas} \tag{S1}$$

where N_{Rh}^{bulk} is the number of atoms in the crystal cell of the bulk structure. The calculated Rh bulk cohesive energy is -6.150 eV/atom. The relaxation energy (E_{relax}) as function of the coordination number is calculated by fitting DFT relaxation energies with the formula proposed by Chang et al.[1]. The DFT relaxation energies are obtained by periodic slab calculations. For each slab, first all the atoms are held fixed at distances of the fcc bulk. Then, one atom with the desired coordination number is allowed to relax. The difference in energy between the first and the second structure gives the relaxation energy for the considered coordination number. The slabs employed for the study are: Rh(100) for CN_8, Rh(110) for CN_7 and CN_{11}, Rh(111) for CN_9, Rh(210) for CN_6 and CN_{10}, Rh(111) with one Rh atom in the fcc site for CN_3, Rh(100) with one and two Rh atoms in the hollow site for CN_4 and CN_5, respectively. The formula proposed by Chang et al.[1] has only one parameter, which for Rh slabs resulted equal to 2.68:

$$E_{relax,i}(CN_i) = \frac{E_{coh}^{bulk}}{12}\left\{\frac{2}{1 + \exp\left[\frac{(12 - CN_i)}{8\,CN_i}\right]}\right\}^{-2.68} \tag{S2}$$

In Figure S1 are reported the DFT relaxation energies (cross-points) and the fitted equation (dotted line).
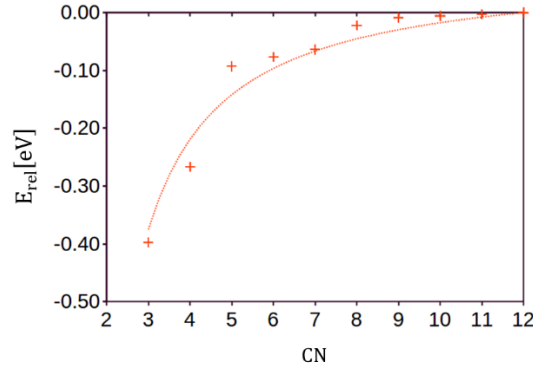
Figure S1: DFT relaxation energies (pluses) and fitted equation proposed by Chang et al.[1] (dotted line).

The strain energy density, W_{strain} inside multiply-twinned particles (MTP) is calculated as function of the shear modulus, μ, and the Poisson's ratio, ν, with the formulas reported by Howie and Marks[2]. Indeed, for the decahedra structures we have:

$$W_{strain}^{dec} = 1.05 \; 10^{-4} \; \mu/(1 - \nu) \tag{S3}$$

And for icosahedra structures:

$$W_{strain}^{ico} = 8.41 \; 10^{-4} \; \mu \, (1 + \nu)/(1 - \nu) \tag{S4}$$

The calculated shear modulus for bulk Rh is 151 GPa, the Poisson's ratio is 0.26. The strain energy per atom (E_{strain}) is obtained by multiplying the strain energy density and the volume of one atom in the fcc bulk, v_{atom}:

$$E_{strain} = W_{strain} v_{atom} \tag{S5}$$

The twin boundary energy of MTPs, E_{twin}, is calculated with a supercell characterized by an inversion of the bulk symmetry along the (111) direction, represented in Figure S2. The cell contains two symmetric planes, therefore the twin boundary energy per atom is calculated as:

$$E_{twin} = \frac{1}{2}\left[E_{DFT}^{slab} - 6 \; E_{DFT}^{bulk}\right] \tag{S6}$$

For Rh we obtain a value of E_{twin} of 0.0081 eV/atom.
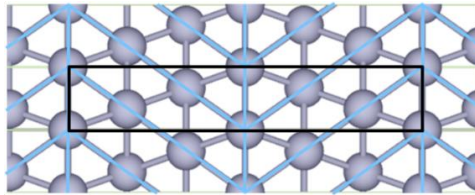
Figure S2: Supercell for calculating the twin boundary energy along the (111) direction. In black is enlightened the cell.

The binding energy of CO at zero coverage ($E_{bind,i}^{0,CO^*}$) is investigated with calculations on the following slab supercells: Rh(100), Rh(110), Rh(111), Rh(210), Rh(211), Rh(311), Rh(321), Rh(331). Moreover, to study adsorption on low coordinated Rh atoms we employ: a Rh(100) slab with one Rh atom in the hollow site (CN_4), a Rh(111) slab with one Rh atom (with CN_3) and three Rh atoms (with CN_5) in the fcc sites. Interestingly, for coordination numbers lower than 5, CO* molecules do not adsorb perpendicular to the slabs but tilted. The binding energy at zero coverage is then corrected with the correlation proposed by Mason et al.[3], with the following formula:

$$\Delta E(\nu_{CO}) = 0.45 - \frac{0.4}{2100 - 1600}(\nu_{CO} - 1600) \tag{S7}$$

where ΔE is the correction applied to correct the CO binding energy and ν_{CO} is the frequency of the CO stretching. As represented in Figure S3, the correction energy differs relevantly for different adsorption sites.
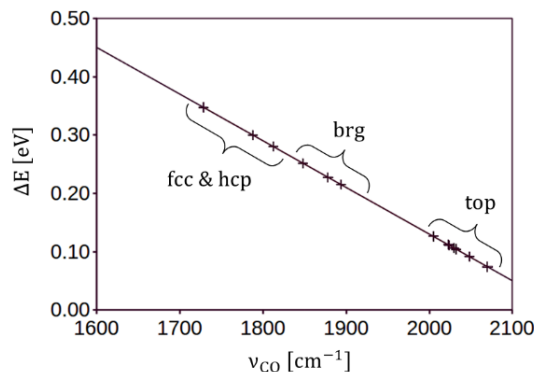

Figure S3: Plot of correction applied to the CO binding energy, function of the CO stretching frequency, according to Mason et al.[3]. With pluses are indicated CO frequencies and corresponding energy corrections for the adsorption sites considered in the work.

A linear correlation between the binding energy at zero coverage (on the top sites) $E_{bind,i}^{0,CO^*}$ and the coordination number (represented in Figure S4) is found:

$$E_{bind,i}^{0,CO^*}(CN_i) = -1.836 + 3.494 \cdot 10^{-2}\, CN_i \tag{S8}$$

Then, the correlation is tested in representing the binding energy on surface atoms of nanoclusters. For clusters with number of atoms higher than 80, the correlation works well. In particular, we test the adsorption of CO* on 3 sites (with CN_3, CN_6 and CN_7) of Rh_{87} and 4 sites (with CN_5, CN_7, CN_8 and CN_9) of Rh_{147}. As represented in Figure S4, we found errors lower than 0.07 eV/CO*.
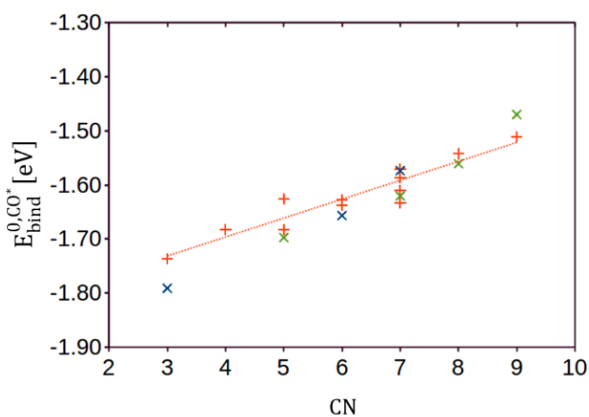
Figure S4: Binding energy of CO as function of the coordination number of the Rh atom at which it is bonded (on the top site). With red pluses are reported the data obtained on periodic surfaces; with crosses are indicated the data obtained on nanoparticles (Rh_{87} in green, Rh_{147} in blue).

The adsorbate-adsorbate interaction, $\Delta E_{bind}^{CO^*}$, is investigated calculating the binding energy at different coverages on 8 Rh crystal facets: Rh(100), Rh(110), Rh(111), Rh(210), Rh(211), Rh(311), Rh(321), Rh(331). We observed that when CO* interacts with neighbor molecules, they relax their positions and tilt the adsorption angle to maximize their distances (maintaining almost the same bond length with the Rh atoms). On all the investigated crystal facets, the relaxed structures at high CO* coverage present similar distorted centered-hexagonal patterns, represented in Figure S5.
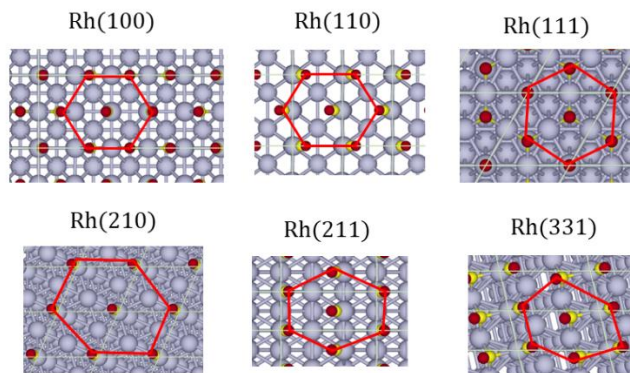
Figure S5: high CO* coverage structures on 6 different crystal facets of Rh. In red are enlightened the distorted centered-hexagonal patterns.

As the adsorbed CO* tend to occupy all the available surface area of the crystal facets, we investigate how their binding energy changes with respect to the ratio between the number of adsorbed CO* molecules (N_{CO^*}) and the total surface area available for adsorption (S_{tot}). We find a good correlation between $\Delta E_{bind}^{CO^*}$ and N_{CO^*}/S_{tot} and we use a power law to describe it:

$$\Delta E_{bind}^{CO^*}(N_{CO^*}/S_{tot}) = 3.034 \cdot 10^{+2} \, (N_{CO^*}/S_{tot})^{3.31} \tag{S9}$$

The two parameters of the power law are fitted on periodic slab calculations (pluses in Figure S6). Then, the correlation is tested on nanocluster at high coverage (crosses in Figure S6). For nanocluster and nanoparticles, S_{tot} is calculated with the following procedure. First, we create a convex hull connecting all the surface atoms (with coordination number lower than 12) and we draw a 3D surface which contains all of them. Then, we enlarge such surface by increasing the distance of each of its point by the average bond length of CO* on Rh facets and we calculate the area of the resulting surface.
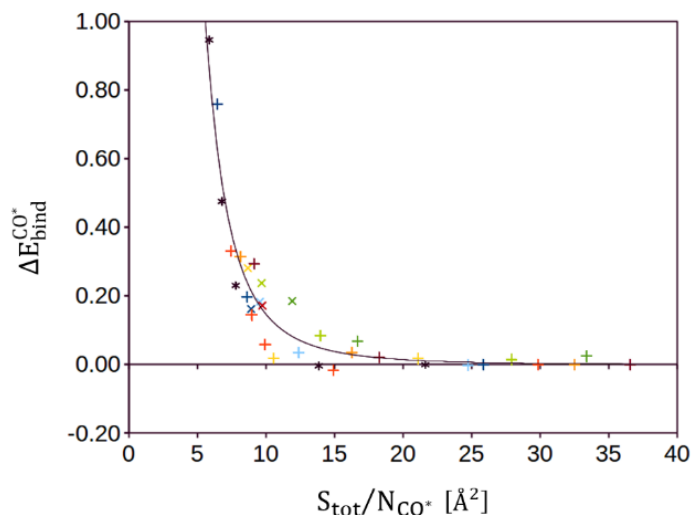
Figure S6: Binding energy difference induced by lateral interaction as function of the average area available to CO* molecules on Rh slabs (pluses) and nanocluster (crosses). With stars are reported the values of CO molecules in vacuum, obtained with hexagonal unit cells with a height of 12 Å.

The contribution of vibrational and translational free energy of adsorbed CO* molecules to the binding, ($\Delta G_i^{CO^*}$) is calculated with slab models at low coverage and the hindered translator model[4]. An average diffusion barrier of CO* molecules (0.12 eV) is employed in the analysis. For each surface slab, $\Delta G_i^{CO^*}$ is evaluated with the following procedure. First, we calculate

the vibrational modes and the corresponding vibrational free energy of the first layer of the clean slab. Then, we calculate the vibrational and translational free energy of the slab with adsorbed CO*, evaluating the vibrational modes of the adsorbate along with the first layer of Rh atoms. $\Delta G_i^{CO^*}$ is obtained as difference between the vibrational and translational free energy of the slab with the adsorbed CO* and the vibrational free energy of the clean slab. As for the binding energy at zero coverage, we find a good correlation between $\Delta G_i^{CO^*}$ and the coordination number of the Rh atom at which CO* is bonded. For the system at 823 K, the correlation obtained (represented in Figure S7.a) is the following:

$$\Delta G_i^{CO^*}(CN_i) = -0.869 + 2.770 \cdot 10^{-2} \, CN_i \qquad (S10)$$

The Gibbs binding energy as a function of the coordination number is then calculated with Equation (7). As an example, for the system at 823 K and P_{CO} = 1 atm ($\Delta\mu_{gas}^{CO}$ = -1.8 eV), we obtain the following correlation (represented in Figure S7.b):

$$G_{bind,i}^{CO^*}(CN_i) = -1.124 + 6.276 \cdot 10^{-2} \, CN_i \qquad (S11)$$

The chemical potential of CO in the gas phase, $\Delta\mu_{gas}^{CO}$, is calculated in the ideal gas approximation:

$$\Delta\mu_{gas}^{CO}(T, P_{CO}) = \Delta\mu_{gas}^{0,CO}(T) + k_B T \ln(P_{CO}/P_0) \qquad (S12)$$

where $\Delta\mu_{gas}^{0,CO}$ is obtained from NASA coefficients[5], and P_0 is the reference pressure, equal to 1 atm.

Figure S7: (a) Contribution of vibrational and translational free energy of adsorbed CO* molecules to the binding ($\Delta G_i^{CO^*}$) at 823 K, as a function of the coordination number of the Rh atom where CO is bonded (on the top site). (b) Gibbs free energy of CO binding (at 823 K and P_{CO} = 1 atm) as a function of the coordination number. The data are obtained on periodic surfaces.

The diffusion barriers required by the hindered translator model[4] are obtained through Climbing-Image Nudged Elastic Band (CI-NEB) calculations, in which the CO* adsorbates move from a preferred adsorption site to a neighbor one (top sites). We calculate the diffusion barriers on Rh(100), Rh(110), Rh(111), Rh(311), Rh(331) and Rh(210) facets and we find that the barriers are similar on all these different facets. Their values range from 0.10 eV to 0.15 eV. The data are shown in Figure S8. Since we did not find any trend between the diffusion barriers and the coordination numbers of the facets, we used an averaged value in our analysis (0.12 eV).
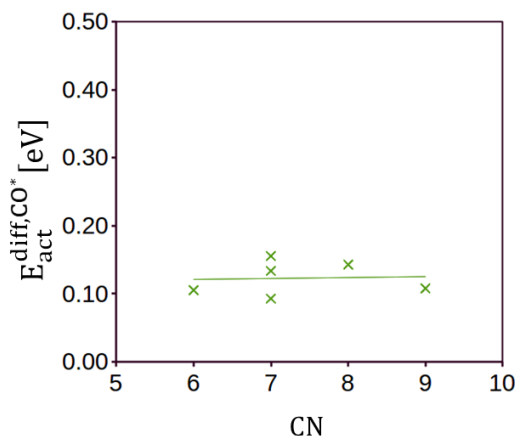
Figure S8: Activation energies of CO* surface diffusion as a function of the coordination number of the Rh atom where CO is bonded (on the top site). The data are obtained on periodic surfaces.

To assess the hindered translator model[4] is really necessary in our work, we calculate $\Delta G_i^{CO^*}(CN_i)$ (the free energy of adsorbed CO using different vibrational entropy contributions) using the simpler harmonic oscillator model (at 823 K) and we compare it with $\Delta G_i^{CO^*}(CN_i)$ obtained using the hindered translator model at the same temperature. The comparison is showed in Figure S9. The difference between the values calculated with the two models is about 0.05 eV per CO molecule (it is almost constant with the coordination number). At higher temperature, we expect this difference to increase, as the behavior of CO* adsorbates approaches that of 2D ideal gases.

Regarding energy deviations, when we tested our model to reproduce the DFT formation energies (Figure 2), we calculated the error to be lower than 0.04 eV per Rh atom. When we compared the binding energies of the model (Equation S8) to our DFT calculations, the error of the model was lower than 0.07 eV per CO molecule, as reported in Figure S4. The difference in the free energies calculated with the harmonic approximation vs the hindered translator (0.05 eV per CO molecule) is of the same order as the errors of the model. As a result, both the accuracies of electronic energy and entropy are relevant for the evaluation of the Gibbs free energies of the nanoparticles in the presence of adsorbed CO.

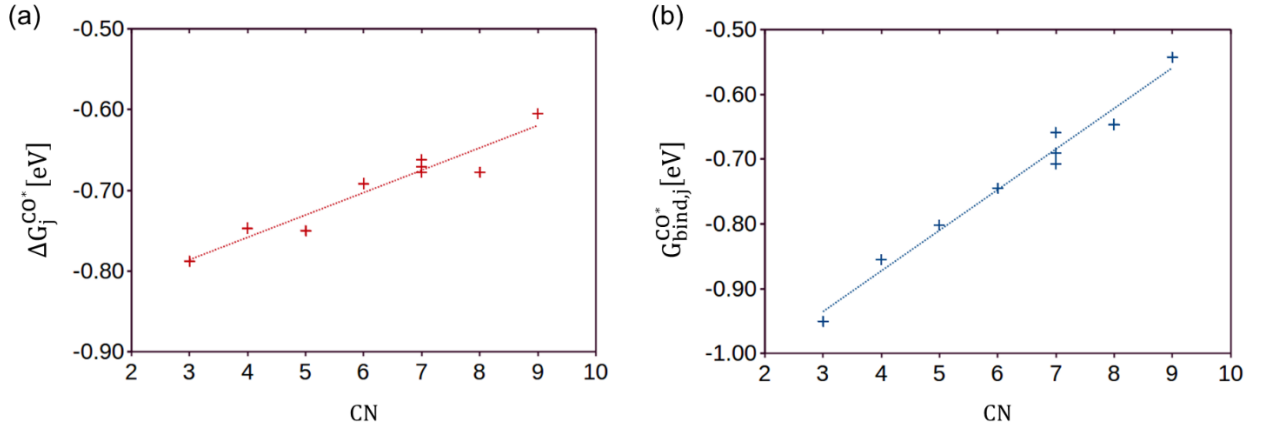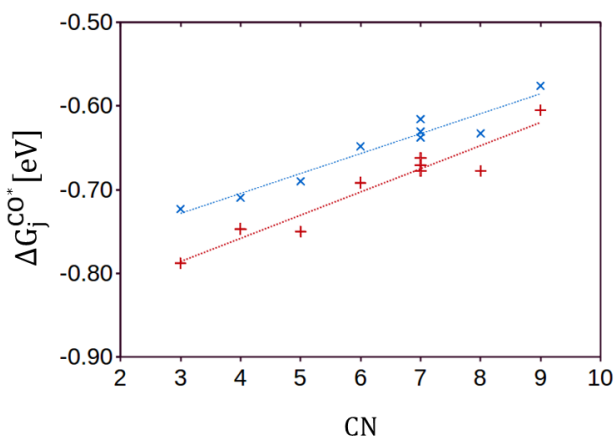**Figure S9:** Contribution of vibrational and translational free energy of adsorbed CO* molecules to the binding ($\Delta G_i^{CO^*}$) at 823 K, as a function of the coordination number of the Rh atom where CO is bonded (on the top site), calculated with the hindered translator model (in red) and the harmonic oscillator model (in blue).

slabs															
Structure	N Rh	CN											E f DFT	E f MOD	Error MOD
	[-]	3	4	5	6	7	8	9	10	11	12	[eV/Rh]	[eV/Rh]	[%]
Rh(100)	7						2				5	0.306	0.309	1.07%
Rh(110)	10					2				2	6	0.307	0.328	6.80%
Rh(111)	7							2		2	5	0.227	0.227	-0.01%
Rh(210)	16			2			2			2	10	0.320	0.344	7.39%
Rh(211)	15					2	2	2			9	0.347	0.360	3.72%
Rh(311)	10					2		2			6	0.364	0.381	4.76%
Rh(321)	22			2			2	2	2	2	12	0.376	0.396	5.33%
Rh(331)	15					2	2		2		9	0.308	0.325	5.54%
Rh(111)+1Rh	30	2					2	6			20	0.313	0.337	7.43%
Rh(111)+2Rh	46		4				2	8	2		30	0.310	0.343	10.47%
Rh(111)+3Rh	69			6			6	6	6		45	0.292	0.313	7.18%
Rh(111)+4Rh	71		4	4			2	10	4		47	0.302	0.321	5.97%
Rh(111)+6Rh	96		4	4	4		2	12			70	0.290	0.295	1.69%
Rh(100)+1Rh	30		2				8				20	0.340	0.370	9.10%
Rh(210)+1Rh	18			2		2	2			2	10	0.446	0.463	3.85%

wires															
Structure	N Rh	CN											E f DFT	E f MOD	Error MOD
	[-]	3	4	5	6	7	8	9	10	11	12	[eV/Rh]	[eV/Rh]	[%]
Rh WIR 030	30					6	2	8			14	0.565	0.561	-0.58%
Rh WIR 058	58					6	2	16			34	0.404	0.400	-1.04%

fcc nanoparticles															
Structure	N Rh	CN											E f DFT	E f MOD	Error MOD
	[-]	3	4	5	6	7	8	9	10	11	12	[eV/Rh]	[eV/Rh]	[%]
Rh FCC 055	55			12		24	6				13	1.215	1.178	-3.06%
Rh FCC 075	75		4	20			33				18	1.170	1.164	-0.54%
Rh FCC 079	79				24	12		24			19	1.007	0.970	-3.67%
Rh FCC 087	87		8		24	12			24		19	1.049	1.053	0.37%
Rh FCC 135	135				48			24	8	12	43	0.887	0.868	-2.08%
Rh FCC 140	140				26	24		48			42	0.820	0.827	0.75%
Rh FCC 147	147			12		48	24	8			55	0.850	0.839	-1.33%
Rh FCC 157	157		4		28	28	16	16	2	12	51	0.823	0.829	0.79%
Rh FCC 165	165			24		48	6	8		36	43	0.810	0.833	2.86%
Rh FCC 225	225			24	24	36	6		48		87	0.754	0.760	0.86%
Rh CUB 147	147	4		28			65				50	0.952	0.941	-1.22%

multiply twinned nanoparticles															
Structure	N Rh	CN											E f DFT	E f MOD	Error MOD
	[-]	3	4	5	6	7	8	9	10	11	12	[eV/Rh]	[eV/Rh]	[%]
Rh DEC 055	55			10	7	10	15				13	1.180	1.153	-2.32%
Rh DEC 127	127				22	30	10	10	15		40	0.869	0.846	-2.64%
Rh DEC 136	136				32		35	20	5		44	0.862	0.830	-3.76%
Rh DEC 146	146				22	20	20	30	5		49	0.830	0.790	-4.80%
Rh DEC 147	147			10	12	20	40	10			55	0.848	0.830	-2.17%
Rh DEC 247	247				22	30	30	60	5		100	0.700	0.667	-4.65%
Rh ICO 055	55			12			30				13	1.177	1.075	-8.69%
Rh ICO 092	92		3	12	9		30	10			28	0.982	0.975	-0.72%
Rh ICO 147	147			12			60	20			55	0.818	0.798	-2.41%
Rh ICO 184	184		4	11	13		49	33			74	0.777	0.784	0.90%
Rh ICO 309	309			12			90	60			147	0.681	0.643	-5.69%

Table S1: Table of the data set of clean slabs, wires and nanoparticles used and analyzed in the work. In the table are reported: the numbers of Rh atoms (N Rh); the distributions of coordination numbers (CN); the formation energies per Rh atom calculated with DFT (E f DFT) and with the model described in the work (E f MOD), Eq. (2); the percentage errors (Error MOD).

slabs						
Structure	CN Rh*	E b DFT	E b MOD	Error MOD	E f DFT	E f MOD
	[-]	[eV/CO]	[eV/CO]	[eV/Rh]	[eV/Rh]	[eV/Rh]
Rh(100)	8	-1.536	-1.556	1.35%	0.196	0.198
Rh(110)	7	-1.583	-1.591	0.55%	0.228	0.248
Rh(111)	9	-1.511	-1.522	0.70%	0.119	0.118
Rh(210)	6	-1.606	-1.626	1.24%	0.220	0.242
Rh(211)	7	-1.632	-1.591	-2.47%	0.238	0.254
Rh(311)	7	-1.602	-1.591	-0.65%	0.203	0.222
Rh(321)	6	-1.617	-1.626	0.59%	0.229	0.248
Rh(331)	7	-1.584	-1.591	0.44%	0.202	0.218
Rh(111)+1Rh	3	-1.672	-1.731	3.56%	0.202	0.221
Rh(111)+2Rh	4	-1.598	-1.696	6.14%	0.241	0.269
Rh(111)+3Rh	5	-1.594	-1.661	4.25%	0.246	0.265
Rh(111)+4Rh	5	-1.673	-1.661	-0.71%	0.255	0.274
Rh(100)+1Rh	4	-1.679	-1.696	1.02%	0.242	0.257
Rh(210)+1Rh	5	-1.641	-1.661	1.22%	0.280	0.279

nanoparticles						
Structure	CN Rh*	E b	E b MOD	Error MOD	E f DFT	E f MOD
	[-]	[eV/CO]	[eV/CO]	[eV/Rh]	[eV/Rh]	[eV/Rh]
Rh FCC 087	3	-1.726	-1.731	0.30%	1.028	1.033
	6	-1.636	-1.626	-0.59%	0.822	0.828
	7	-1.565	-1.591	1.67%	0.832	0.833
Rh FCC 147	5	-1.687	-1.661	-1.54%	0.713	0.703
	7	-1.612	-1.591	-1.29%	0.588	0.579
	8	-1.555	-1.556	0.13%	0.840	0.828
	9	-1.470	-1.522	3.50%	0.771	0.756

Table S2: Table of the data set of CO adsorption at low coverage on slabs and nanoparticles. In the table are reported: the coordination numbers of the Rh atom at which CO is adsorbed (CN Rh*); the binding energies calculated with DFT (E b DFT) and with the model illustrated in the work (E b MOD); the percentage errors (Error MOD); the formation energies of the systems with adsorbed CO* at low coverage calculated with DFT (E f DFT) and with the model (E f MOD).

slabs

Rh(100)

site	CO stretch	N CO top	N CO brg	N CO hol	E b DFT	CORR	E b CORR
[-]	[1/cm]	[-]	[-]	[-]	[eV/CO]	[eV]	[eV]
top	2029.6	1	0	0	-1.508	-0.006	-1.515
brg	1878.1	0	1	0	-1.589	0.109	-1.480

Structure	Stot	N CO top	N CO brg	N CO hol	E b DFT	E b CORR	Stot / N CO*	E b MOD	Error MOD	E f DFT	E f MOD
[-]	[Å²]	[-]	[-]	[-]	[eV/CO]	[eV/CO]	[Å²]	[eV/CO]	[eV/Rh]	[eV/Rh]	[eV/Rh]
clean	7.465	0	0	0						0.306	0.309
0.25 ML top	29.859	1	0	0	-1.508	-1.515	29.859	-1.553	2.48%	0.252	0.254
0.50 ML top	14.930	1	0	0	-1.525	-1.531	14.930	-1.518	-0.90%	0.197	0.201
0.75 ML Gurney	59.718	2	4	0	-1.503	-1.432	9.953	-1.407	-1.76%	0.153	0.159
0.83 ML Yong	89.577	4	6	0	-1.412	-1.349	8.958	-1.345	-0.36%	0.146	0.149
1.00 ML brg	14.930	0	2	0	-1.258	-1.149	7.465	-1.169	1.72%	0.142	0.142

Rh(110)

site	CO stretch	N CO top	N CO sbr	N CO lbr	E b DFT	CORR	E b CORR
[-]	[1/cm]	[-]	[-]	[-]	[eV]	[eV]	[eV]
top	2004.9	1	0	0	-1.631	0.012	-1.618
sbr	1848.0	0	1	0	-1.599	0.132	-1.468

Structure	Stot	N CO top	N CO sbr	N CO lbr	E b DFT	E b CORR	Stot / N CO*	E b MOD	Error MOD	E f DFT	E f MOD
[-]	[Å²]	[-]	[-]	[-]	[eV/CO]	[eV/CO]	[Å²]	[eV/CO]	[eV/Rh]	[eV/Rh]	[eV/Rh]
clean	10.557	0	0	0						0.307	0.328
0.25 ML top	42.227	1	0	0	-1.631	-1.618	42.227	-1.590	-1.73%	0.262	0.284
0.50 ML top	21.114	1	0	0	-1.613	-1.601	21.114	-1.579	-1.35%	0.218	0.240
1.00 ML shift hol	21.114	0	2	0	-1.581	-1.449	10.557	-1.468	1.33%	0.146	0.165

Rh(111)

site	CO stretch	N CO top	N CO fcc	N CO hcp	E b DFT	CORR	E b CORR
[-]	[1/cm]	[-]	[-]	[-]	[eV]	[eV]	[eV]
top	2048.2	1	0	0	-1.478	-0.021	-1.499
fcc	1812.5	0	1	0	-1.440	0.159	-1.281
hcp	1787.6	0	0	1	-1.550	0.177	-1.372

Structure	Stot	N CO top	N CO fcc	N CO hcp	E b DFT	E b CORR	Stot / N CO*	E b MOD	Error MOD	E f DFT	E f MOD
[-]	[Å²]	[-]	[-]	[-]	[eV/CO]	[eV/CO]	[Å²]	[eV/CO]	[eV/Rh]	[eV/Rh]	[eV/Rh]
clean	6.465	0								0.227	0.227
0.25 ML top	25.859	1	0	0	-1.478	-1.499	25.859	-1.515	1.09%	0.164	0.164
0.75 ML mix	25.859	1	1	1	-1.292	-1.187	8.620	-1.281	7.90%	0.079	0.067
1.00 ML top	6.465	1	0	0	-0.789	-0.810	6.465	-0.897	10.77%	0.092	0.077

Rh(210)

site	CO stretch	N CO top	N CO fcc	N CO hcp	E b DFT	CORR	E b CORR
[-]	[1/cm]	[-]	[-]	[-]	[eV]	[eV]	[eV]
top	2052.2	1	0	0	-1.562	-0.024	-1.585

Structure	Stot	N CO top	N CO fcc	N CO hcp	E b DFT	E b CORR	Stot / N CO*	E b MOD	Error MOD	E f DFT	E f MOD
[-]	[Å²]	[-]	[-]	[-]	[eV/CO]	[eV/CO]	[Å²]	[eV/CO]	[eV/Rh]	[eV/Rh]	[eV/Rh]
clean	16.692	0	0	0						0.320	0.344
0.25 ML top	66.767	1	0	0	-1.562	-1.585	66.767	-1.626	2.56%	0.287	0.310
0.50 ML top	33.383	1	0	0	-1.537	-1.561	33.383	-1.624	4.02%	0.255	0.276
1.00 ML top	16.692	1	0	0	-1.493	-1.517	16.692	-1.599	5.44%	0.194	0.211

Rh(211)

site	CO stretch	N CO top	N CO hcp	N CO top 2	E b DFT	CORR	E b CORR
[-]	[1/cm]	[-]	[-]	[-]	[eV]	[eV]	[eV]
top	2022.8	1	0	0	-1.574	-0.001	-1.575
hcp	1728.1	0	1	0	-1.492	0.223	-1.269
top 2	2048.5	0	0	1	-1.387	-0.021	-1.408

Structure	Stot	N CO top	N CO hcp	N CO top2	E b DFT	E b CORR	Stot / N CO*	E b MOD	Error MOD	E f DFT	E f MOD
[-]	[Å²]	[-]	[-]	[-]	[eV/CO]	[eV/CO]	[Å²]	[eV/CO]	[eV/Rh]	[eV/Rh]	[eV/Rh]
clean	18.285	0	0	0						0.347	0.360
0.50 ML top	36.570	1	0	0	-1.574	-1.575	36.570	-1.589	0.91%	0.281	0.294
1.00 ML mix	36.570	1	0	1	-1.459	-1.470	18.285	-1.572	6.87%	0.224	0.229
2.00 ML mix	18.285	1	0	1	-1.256	-1.267	9.142	-1.393	9.95%	0.136	0.128

Rh(311)

site	CO stretch	N CO top	N CO brg	N CO hcp	E b DFT	CORR	E b CORR
[-]	[1/cm]	[-]	[-]	[-]	[eV]	[eV]	[eV]
top	2032.3	1	0	0	-1.541	-0.009	-1.550
brg	1893.6	0	1	0	-1.661	0.097	-1.564

Structure	Stot	N CO top	N CO brg	N CO hcp	E b DFT	E b CORR	Stot / N CO*	E b MOD	Error MOD	E f DFT	E f MOD
[-]	[Å²]	[-]	[-]	[-]	[eV/CO]	[eV/CO]	[Å²]	[eV/CO]	[eV/Rh]	[eV/Rh]	[eV/Rh]
clean	12.379	0	0	0						0.364	0.381
0.25 ML top	49.516	1	0	0	-1.541	-1.550	49.516	-1.591	2.64%	0.315	0.331
0.50 ML top	49.516	2	0	0	-1.543	-1.551	24.758	-1.584	2.12%	0.267	0.282
1.00 ML brg	24.758	0	2	0	-1.626	-1.529	12.379	-1.519	-0.65%	0.172	0.191

Rh(321)

site	CO stretch	N CO top	N CO top 2	N CO brg	E b ave	CORR	E b CORR
[-]	[1/cm]	[-]	[-]	[-]	[eV]	[eV]	[eV]
top	2050.1	1	0	0	-1.590	-0.022	-1.612
top 2	2030.6	0	1	0	-1.564	-0.007	-1.572

Structure	Stot	N CO top	N CO top 2	N CO hcp	E b DFT	E b CORR	Stot / N CO*	E b MOD	Error MOD	E f DFT	E f MOD
[-]	[Å²]	[-]	[-]	[-]	[eV/CO]	[eV/CO]	[Å²]	[eV/CO]	[eV/Rh]	[eV/Rh]	[eV/Rh]
clean	27.931	0	0	0						0.376	0.396
0.50 ML top	55.861	1	0	0	-1.590	-1.612	55.861	-1.626	0.85%	0.331	0.351
1.00 ML top	27.931	1	0	0	-1.575	-1.597	27.931	-1.621	1.51%	0.287	0.306
2.00 ML mix	27.931	1	1	0	-1.494	-1.508	13.965	-1.578	4.61%	0.208	0.221

Rh(331)

site	CO stretch	N CO top	N CO brg	N CO top 2	E b DFT	CORR	E b CORR
[-]	[1/cm]	[-]	[-]	[-]	[eV]	[eV]	[eV]
top	2023.6	1	0	0	-1.492	-0.002	-1.494

Structure	Stot	N CO top	N CO brg	N CO top 2	E b DFT	E b CORR	Stot / N CO*	E b MOD	Error MOD	E f DFT	E f MOD
[-]	[Å²]	[-]	[-]	[-]	[eV/CO]	[eV/CO]	[Å²]	[eV/CO]	[eV/Rh]	[eV/Rh]	[eV/Rh]
clean	16.269	0	0	0						0.308	0.325
0.50 ML top	32.538	1	0	0	-1.492	-1.494	32.538	-1.588	6.33%	0.245	0.258
1.00 ML top	32.538	2	0	0	-1.457	-1.459	16.269	-1.562	7.10%	0.186	0.194
2.00 ML mix	16.269	2	0	0	-1.178	-1.180	8.135	-1.300	10.17%	0.111	0.108

nanoparticles												
FCC 087												
Structure	Area $[A^2]$	N CO CN 3 [-]	N CO CN 6 [-]	N CO CN 7 [-]		E b DFT [eV/CO]	E b CORR [eV/CO]	Stot / N CO* $[Å^2]$	E b MOD [eV/CO]	Error MOD [eV/Rh]	E f DFT [eV/Rh]	E f MOD [eV/Rh]
1.00 ML mix	524.867	8	24	12		-1.448	-1.498	11.929	-1.554	3.72%	0.315	0.277
FCC 147												
Structure	Area $[A^2]$	N CO CN 5 [-]	N CO CN 7 [-]	N CO CN 8 [-]	N CO CN 9 [-]	E b DFT [eV/CO]	E b CORR [eV/CO]	Stot / N CO* $[Å^2]$	E b MOD [eV/CO]	Error MOD [eV/Rh]	E f DFT [eV/Rh]	E f MOD [eV/Rh]
1.00 ML	822.296	12	48	24	8	-1.433	-1.423	8.938	-1.372	-3.56%	-0.046	-0.040
CUB 147												
Structure	Area $[A^2]$	N CO CN 3 [-]	N CO CN 5 [-]	N CO CN 8 [-]		E b DFT [eV/CO]	E b CORR [eV/CO]	Stot / N CO* $[Å^2]$	E b MOD [eV/CO]	Error MOD [eV/Rh]	E f DFT [eV/Rh]	E f MOD [eV/Rh]
1.00 ML	888.219	4	28	65		-1.380	-1.370	9.157	-1.397	1.94%	0.041	0.027

Table S3: Table of the data set of CO adsorption at high coverage on slabs and nanoparticles. For adsorption at a single site, in the table are reported: the frequencies of the CO stretching; the numbers of adsorbed CO*; the binding energies calculated with DFT (E b DFT) and corrected with the formula proposed by Manson et al.[3] (E b CORR). Then, for the systems at high coverage are reported: the total surface of the system (S tot); the number of CO; the average binding energies calculated with DFT and corrected; the ratio between the surface area and the number of CO molecules (Stot / N CO*); the binding energies calculated with the model proposed in the work (E b MOD); the percentage error; the formation energies of the system calculated with DFT (E f DFT) and with the model (E f MOD).

Section 3: Identification of active sites and calculation of reaction rates of CO* dissociation.

An example of catalytic sites grid is reported in Figure S10. The binding sites recognized are: top, bridge, (100)-hollow, (110)-long bridge, (110)-long hollow, (111)-fcc, (111)-hcp, (311)-step and (210)-step.
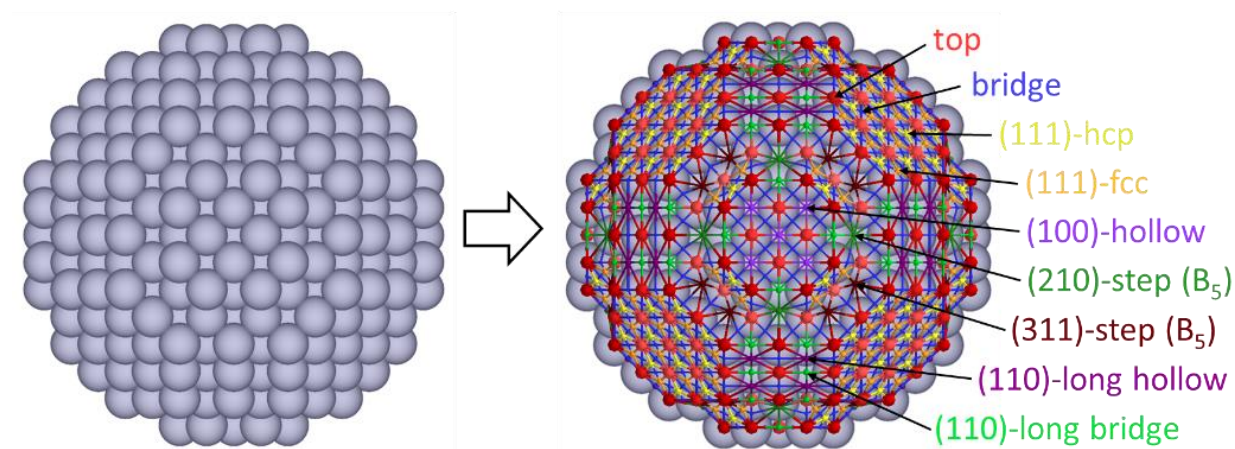

Figure S10: Binding sites grid of one sample nanoparticle. The binding sites recognized are: top (red), bridge (blue), (100)-hollow (violet), (110)-long bridge (green), (110)-long hollow (purple), (111)-fcc (orange), (111)-hcp (yellow), (311)-step (brown) and (210)-step (dark green). Top sites are also differentiated by their coordination number: they are darker with the decrease of their coordination number.

We simulate the reaction path of CO* dissociation on 6 crystal facets of Rh. The geometry of initial, final and transition states are reported in Figure S11. Within harmonic transition state theory, we calculate the Gibbs activation energies of the elementary step on the six facets. The resulting values are reported in Table S1. For the different facets, the transition state is found in correspondence of different active sites. The activation Gibbs free energy for CO* dissociation is affected mostly by the geometry (type) of active site. For the case of B_5 sites, we analyzed the CO* dissociation on three Rh crystal facets with different coordination environments. On Rh(211), the B_5 site is provided by two atoms with CN_{10}, two with CN_7

and one with CN_9. On Rh(311), the B_5 site is provided by two CN_{10} and three CN_7. On Rh(210), the B_5 site is provided by two CN_6, two CN_9 and one CN_{11}. As reported in Table S4, the Gibbs activation energies on the three facets which show B_5 sites are similar, and they are significantly lower than the Gibbs activation energies on the other Rh crystal facets.

Table S4. Gibbs activation energies of the CO* dissociation elementary step on six facets of Rh.

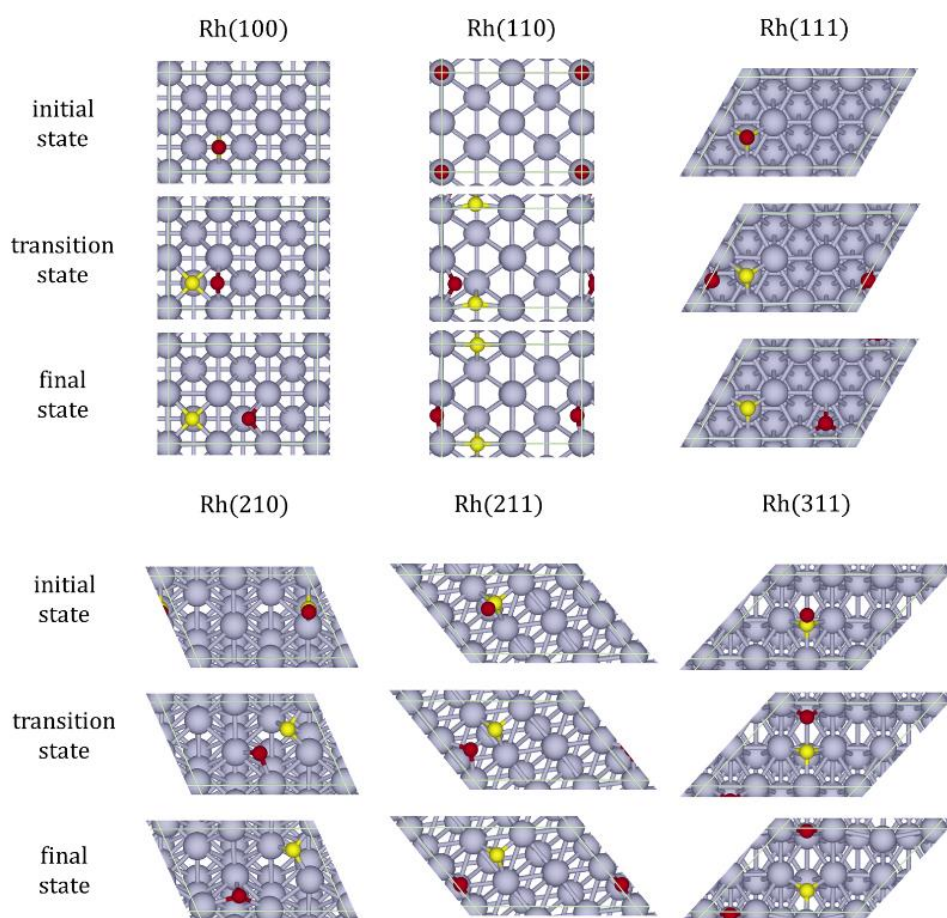| facet	Rh(100)	Rh(110)	Rh(111)	Rh(211)	Rh(311)	Rh(210)
site	hol	lho	fcc	B_5	B_5	B_5
Gact	2.204	2.642	3.117	1.685	1.812	1.775

Figure S11: Geometry of initial states, final states and transition states of CO dissociation elementary step on the six surfaces of Rh: (100), (110), (111), (210), (211) and (311).
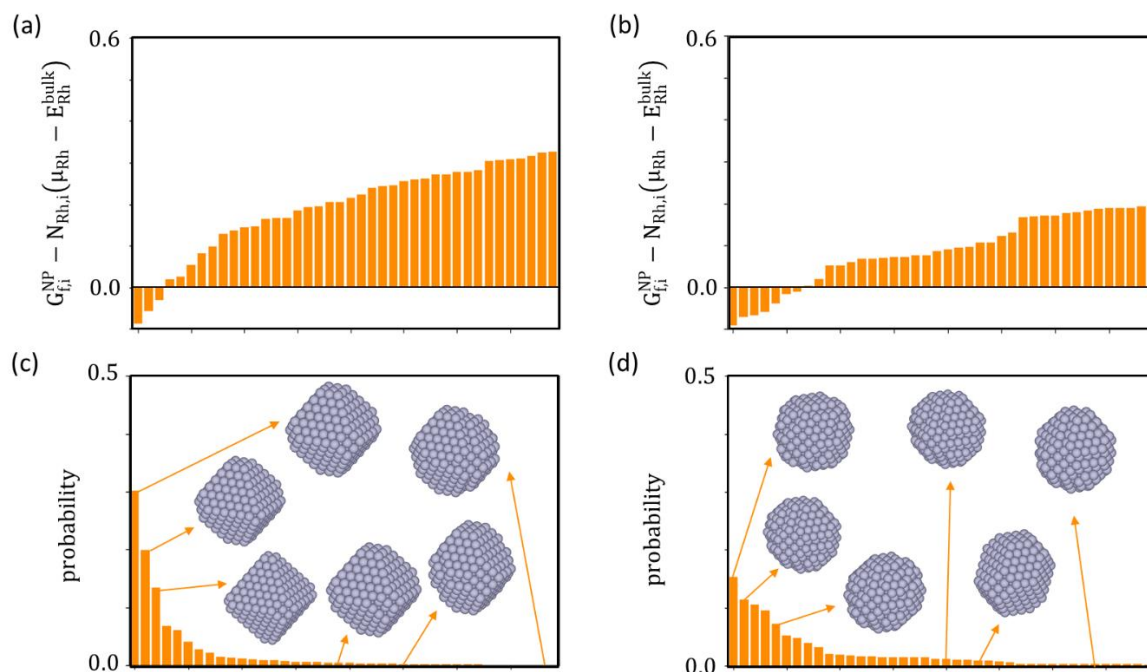
Figure S12: Gibbs formation energies relative to the Rh chemical potential in the system (μ_{Rh}) of the 40 most stable nanoparticles in the ensemble for $P_{CO} = 10^{-3}$ (a) and 10^{-1} atm (b). Nanoparticles' corresponding probability evaluated with a Boltzmann distribution for $P_{CO} = 10^{-3}$ (c) and 10^{-1} atm (d). Examples of nanoparticles with relevant probabilities are represented as insets in the figures.

References:

(1)   Sun, C. Q.; Tay, B. K.; Zeng, X. T.; Li, S.; Chen, T. P.; Zhou, J.; Bai, H. L.; Jiang, E. Y. Bond-Order-Bond-Length-Bond-Strength (Bond-OLS) Correlation Mechanism for the Shape-and-Size Dependence of a Nanosolid. *J. Phys. Condens. Matter* **2002**, *14* (34), 7781–7795. https://doi.org/10.1088/0953-8984/14/34/301.

(2)   Howie, A.; Marks, L. D. Elastic Strains and the Energy Balance for Multiply Twinned Particles. *Philos. Mag. A Phys. Condens. Matter, Struct. Defects Mech. Prop.* **1984**, *49* (1), 95–109. https://doi.org/10.1080/01418618408233432.

(3)   Mason, S. E.; Grinberg, I.; Rappe, A. M. First-Principles Extrapolation Method for Accurate CO Adsorption Energies on Metal Surfaces. *Phys. Rev. B - Condens. Matter Mater. Phys.* **2004**, *69* (16), 1–4. https://doi.org/10.1103/PhysRevB.69.161401.

(4)   Sprowl, L. H.; Campbell, C. T.; Árnadóttir, L. Hindered Translator and Hindered Rotor Models for Adsorbates: Partition Functions and Entropies. *J. Phys. Chem. C* **2016**, *120* (18), 9719–9731. https://doi.org/10.1021/acs.jpcc.5b11616.

(5)   Mcbride, B.; Gordon, S.; Reno, M. Coefficients for Calculating Thermodynamic and Transport Properties of Individual Species. *Nasa Tech. Memo.* **1993**, *4513* (NASA-TM-4513), 98.